Title
CHARACTERISTICS OF INFRARED SKY RADIATION IN THE UNITED STATES

Authors
Martin, M.
Berdahl, P.

Publication Date
1983-07-01

LBL-16344
Preprint

Lawrence Berkeley Laboratory

UNIVERSITY OF CALIFORNIA

APPLIED SCIENCE DIVISION

Submitted to Solar Energy

CHARACTERISTICS OF INFRARED SKY RADIATION IN THE UNITED STATES

M. Martin and P. Berdahl

July 1983

APPLIED SCIENCE DIVISION

Prepared for the U.S. Department of Energy under Contract DE-AC03-76SF00098

DISCLAIMER

CHARACTERISTICS OF INFRARED SKY RADIATION IN THE UNITED STATES*

Marlo Martin and Paul Berdahl
Lawrence Berkeley Laboratory
University of California
Berkeley, CA 94720

ABSTRACT

A new algorithm has been developed for calculating the thermal radiant temperature of the sky. It is based on a simple empirical and theoretical model of clouds, together with a correlation between clear sky emissivity and the surface dewpoint temperature. Hourly sky temperatures have been calculated based on Typical Meteorological Year (TMY) weather data sets. A summary of the results is presented for calculations made at 193 TMY sites within the continental United States. The results are displayed in the form of monthly contour maps, histograms, and graphs for the purpose of determining regions of the country in which the radiative cooling of buildings appears to be a promising heat rejection strategy.

1. *INTRODUCTION*

Infrared heat transfer between building surfaces and the sky is usually treated in a very approximate manner due to the difficulty in finding reliable measured data for the apparent sky emissivity or sky temperature[1]. Some passive cooling systems make use of the lower effective radiant temperatures of the sky at night as a means of rejecting excess heat[2]. Likewise, the prediction of solar collector performance is improved if accurate infrared sky radiation values are available. Freezing problems in liquid collectors are brought about by the combined effect of air temperature and sky temperature, as are the natural formation processes for dew, frost, and ground fog.

Results of a spectral infrared sky radiance measurement program have recently been reported by our group for six U.S. cities[3]. The results have shown that the clear sky emissivity can be predicted accurately as a function of the dewpoint temperature, with no apparent systematic variations due to location within the continental United States. Corrections to the clear sky emissivity can be made if the fractional cloud cover and cloudbase temperatures are also known. This information is all available, in various approximations, on weather tapes maintained by the U.S. National Climatic Center in Asheville, NC. The approach taken in the present study has been to develop a

*This work was supported by the Assistant Secretary for Conservation and Renewable Energy, Office of Solar Heat Technologies, Passive and Hybrid Solar Energy Division of the U.S. Department of Energy under Contract No. DE-AC03-76 SF00098

computer algorithm based on our radiometer measurements, and to use this algorithm with hourly weather data obtained from 193 Typical Meteorological Year tapes to calculate mean sky temperature depressions and histograms for the continental United States.

In Section 2 we describe the algorithm used to derive the sky emissivity and sky temperature from the hourly weather data available on TMY tapes. Section 3 is devoted to a comparison of monthly averages of the calculated sky emissivity with measurements made by our spectral infrared radiometer. The results of the sky temperature calculations are then summarized in the remaining Sections. Contour maps are developed for the average monthly sky temperature depression (Section 4) and for the monthly distribution of summertime "cool" sky temperature below 16°C (Section 6). In Section 5 it is shown that the apparent sky temperature depression for a selective radiator is a constant multiple of this quantity as measured by a blackbody surface, as developed in Section 4. In Section 7 we present histograms showing the monthly distribution of the sky temperature depression for the five warmest months of the year. And finally, we show graphs indicating the cumulative percentage of monthly hours for which the sky temperature falls below values of 10 to 26°C (50° to 79°F).

2. *SKY EMISSIVITY ALGORITHM*

2.1. *Clear Sky Emissivity*

The monthly average clear sky emissivity is first obtained as a function of the dewpoint temperature T_{dp} (°C) using the relationship[4],

$$\epsilon_o = 0.711 + 0.56 \left(\frac{T_{dp}}{100}\right) + 0.73 \left(\frac{T_{dp}}{100}\right)^2 . \qquad (1)$$

In order to use this equation for predicting hourly emissivities, an approximate diurnal correction is added[5]:

$$\Delta \epsilon_h = 0.013 \cos \left[2\pi \frac{t}{24}\right] \qquad (2)$$

where t is the hour of the day. An additional correction is added to adjust for the elevation of the observing station[6]:

$$\Delta\epsilon_e = 0.00012\,(P-1000), \tag{3}$$

where P is the station pressure in millibars.

2.2. *Sky Emissivity in the Presence of Clouds*

The presence of cloud cover increases the total sky emissivity above the clear sky value. We express this relationship in the form:

$$\epsilon = \epsilon_o + (1-\epsilon_o)C \tag{4}$$
$$\text{and} \quad C = n\epsilon_c\,\Gamma\ ,$$

where ϵ_o is the clear sky emissivity, n is the fractional area of the sky covered by clouds, ϵ_c is the hemispherical cloud emissivity, and Γ is a factor depending on the cloud height h. The parameter C is the "infrared cloud amount". The cloud factor Γ is expected to be small for high (cold) clouds, and to approach unity for low clouds. In order to obtain the functional form of Γ (h) we have calculated ϵ_o for clear skies and ϵ for an opaque ceiling ($n = 1.0$ and $\epsilon_c = 1.0$) at various ceiling heights h using the LOWTRAN computer program for four model atmospheres [7]. The cloudbase is simulated as a blackbody emitter.

The results are plotted in Figure 1 for the quantity

$$\Gamma(h) = \frac{\epsilon-\epsilon_o}{1-\epsilon_o}\ .$$

The expression for total clear sky emissivity (Eq.1) can be generalized to include contributions from cloud layers at different heights h_i:

$$\epsilon = \epsilon_o + (1-\epsilon_o)\sum_i n_i\epsilon_{c,i}\,\Gamma(h_i) \tag{5}$$

The cloud fractions n_i are those visible to an observer on the ground. For example, if the fraction of low clouds is 0.7, the maximum fraction of upper clouds is 0.3. Low and mid-level clouds tend to be opaque ($\epsilon_{c,i} \approx 1.0$), while a great deal of variation is observed in the emissivity of cirrus clouds. Platt and Dilley [8] reported on measurements of the vertical beam emissivities of cirrus cloud systems. Using their data for 22 observations, converted from beam to hemispherical cloud emissivities*, we plot the observed emissivity as a function of cloudbase height in Figure 2.

*The formula $\epsilon_c \approx 1 - (1-\epsilon_c^{beam})^{1.66}$ was used to convert from beam to hemispherical emissivities. Additional refinements to this equation could be introduced, but the scatter of points in Figure 2 suggests that such an ap-

Although the solid line represents a least squares fit between 4 and 11 kilometers, considerable variation is observed in the infrared emissivity from cirrus cloud systems.

The cloud factor Γ used here has been established as a function of cloud height. A more accurate procedure would be to define it in terms of the difference between the air temperature at the ground and the cloud base temperature $\Delta T_c = T_{air} - T_{cloud}$. Using the results of the same LOWTRAN calculations from which Figure 1 was generated, one obtains the relationship

$$\Gamma(\Delta T_c) = exp(-\Delta T_c / \Delta T_o) \quad , \tag{6}$$

where $\Delta T_o = 46^o C\ (83^o F)$, which is shown in Figure 3. The closeness of the fit confirms that Equation (6) is superior for estimating Γ as compared to using the functional form shown in Figure 1. However, since cloudbase temperatures are usually not available, we have used the expression $\Gamma(h) = \exp(-h/h_o)$ in the work reported here. The two equations are equivalent if a lapse rate of 5.6^oC per km is assumed.

One implicit assumption is the assertion that the sky emissivity is a linear function of the fraction of cloud cover estimated by a visual observer. It is possible, for example, to replace n_l in Eq. (5) with n_l^α, where α is a numerical value. The resulting sky emissivity would be identical in all cases where $n_l = 0$ or 1, but would differ for intermediate values. The motivation for seeking a more general relationship is that under broken cloud cover the infrared and visual cloud amounts need not be identical. For example, if $n_l = 0.2$ one expects to find scattered clouds near the horizon and little difference between the total sky emissivity and the clear sky value. Thus, α must be greater than one to ensure that $n_l^\alpha < n_l$. This refinement, however, is beyond the scope of our current treatment. Fortunately it is also not necessary due to the size of other errors in the model (especially for ϵ_o), and the fact that the cloud cover is frequently near 0 or 1, for which the error vanishes.

Once the total sky emissivity has been calculated, the sky temperature depression is readily obtained from the equation

---

proach would not lead to increased accuracy.

$$\Delta T_s = T_{air} - T_{sky} = (1 - \epsilon^{1/4})\ T_{air} \qquad (7)$$

where T_{air} is the ambient drybulb temperature expressed in degrees Kelvin.

2.3. *Sky Emissivity Algorithm for TMY Weather Data*

Typical Meteorological Year (TMY) weather tapes were selected as a source of hourly climatic data. These tapes are available for 234 locations throughout the United States, of which 211 sites are in the continental 48 states. The clear sky emissivity is first calculated by means of Equations 1 to 3.

Estimation of the contribution of cloud cover to the infrared sky emissivity is complicated by the fact that all the information required by Equation 5 is not recorded in the TMY format. The available hourly data consists of the amount of opaque and total sky cover in tenths, ceiling height whenever the opaque sky cover exceeds or equals 0.6, and a sky condition indicator which gives limited information on the thickness and opacity of up to four cloud layers. The recorded information on cloud height is provided only if an opaque ceiling exists. A default cloud height of 2 km is assigned to opaque clouds.

To make use of this data we have adopted the following procedure. Thin clouds (usually cirrus) are assumed to have an average emissivity of $\epsilon_{c,i} = 0.4$ (see Figure 2). The amount of thin cloud coverage is given by the total cloud cover minus the opaque cloud cover, $n_{thin} = n_{total} - n_{opaque}$. We further assume, for lack of recorded information, that all thin clouds are high clouds to which we assign a default height of $h_i = 8km$.

Whenever an opaque ceiling is recorded, we assume that the base height of all the opaque clouds is at that value. In the event that no ceiling height is defined, we assume that all opaque clouds have a default base height of 2 km. Whenever a cirroform ceiling of indeterminate height is indicated, it is possible that all opaque clouds could be high or that some could exist at lower levels. In this case the sky condition field is read from the tape to determine if more than one cloud layer has been observed. If only a single layer is recorded, it is regarded as being opaque ($\epsilon_{c,i} = 1.0$) at a default height of 8 km. If two or more layers are recorded, the condition of the lower layer is decoded to determine its opacity ($\epsilon_{c,i} = 1.0$ for opaque clouds, $\epsilon_{c,i} = 0.4$ for thin clouds), and the

approximate sky fraction obscured by the layer.

3. *COMPARISON OF CALCULATED AND MEASURED SKY EMISSIVITIES*

The algorithm for calculating the sky emissivity described in Section 2 will be used with hourly TMY weather data to generate monthly sky temperature statistics in Sections 4 through 7. The validity of the algorithm is ultimately based on measurements made over a two year period at six U.S. locations [3], and on LOWTRAN computer model estimates of the radiative effects of cloud cover. In order to estimate the probable accuracy of this method it is desirable to obtain a direct comparison between the measured monthly average sky emissivity values and the results of applying the algorithm of Section 2 using TMY weather data.

Such a direct comparison is complicated by four possible sources of error. First, while the monthly measured values were obviously recorded during a particular month (in 1979 or 1980), it is very unlikely that the weather parameters to which sky emissivity is most sensitive (namely, dewpoint temperature and fractional sky cover) are identical to those of the month appearing in the TMY data set. Second, sky emissivity measurements for the 57 months of recorded data are not always complete for a given month. In some cases this discrepancy is due to an instrument being placed in operation or removed from the site during the middle of the month. In other cases it is due to equipment problems, such as malfunction of a rain sensor, radiometer detector failure, or various mechanical problems. At other times, data was recorded but could not pass rigid quality control tests, and is thus not included in the final data base. Thus, the percentage of hours for which data was recorded (completeness) differs for each of the 57 months.

The remaining two possible error sources are the average instrumental measurement error and the representativeness of the sky emissivity calculated from TMY data with respect to the average of this quantity calculated using hourly weather data over a long time period ($>$ 10 years). The latter question can only be addressed by calculating the hourly sky emissivity over a period of many years and comparing its average to the value obtained from TMY calculations. We make the assumption that the monthly average sky emissivity calculated using the TMY data set adequately represents the

long term average of the same quantity calculated using hourly weather data over a period of many years.

In order to address the first of these sources of error we have developed a simplified technique for calculating the monthly average sky emissivity based on the average monthly dewpoint temperature and fractional sky cover (see Appendix). Emissivities have been calculated in this manner over a period of 15 years for comparison with the same quantity calculated from TMY data. The difference between the monthly TMY emissivity and the average of emissivities calculated by the simplified method typically lies within one standard deviation of the scatter throughout the 15 year Local Climatological Data (LCD) interval. While this standard deviation varies with the month and location, its average value is less than $\delta\epsilon_{(TMY-LCD)} = \pm 0.02$ at the three sites for which such calculations have been made. This provides a measure for the reliability of the simplified LCD calculations of total monthly sky emissivity.

The inaccuracy resulting from incomplete months of measured sky emissivity data is reduced by selecting only the subset of measurements for which the record is more than 60% complete. A comparison of the measured monthly sky emissivity and the values calculated using TMY and LCD weather data is shown in Table 1 for the 27 months satisfying this completeness criterion. The emissivities calculated using the LCD data correspond to the same month and year as the measured values, whereas the TMY emissivity is calculated from a historical month of data that is representative of long term average climate conditions. The measured values were obtained using the procedure described in section 4 of reference [3]. An upper bound can now be placed on the reliability of the calculated monthly sky emissivities for predicting the true measured values by computing the standard deviations between the respective measured and calculated quantities. The standard deviation of the TMY emissivity from the average measured values for the 27 data months is $\delta\epsilon_{TMY} = \pm 0.038$. The corresponding LCD value is $\delta\epsilon_{LCD} = \pm 0.026$. Since part of this error is attributable to inaccuracies inherent in the computational algorithm, and part is due to the instrumental measurement error, the standard deviation of the "exact" measured monthly sky emissivity

from the LCD calculation is less than 0.026.

This inaccuracy can be expressed in terms of the sky temperature uncertainty (taking $T_{air} = 300^{o}K$ and $\epsilon = 0.8$), which corresponds to $\delta T_{sky} = \pm 2.3^{o}C$. On the basis of this analysis we estimate that the expected error in the monthly average sky temperatures to be plotted in the subsequent sections is less than about 2^{o}C.

4. *MONTHLY AVERAGE SKY TEMPERATURE DEPRESSION*

The average monthly depression of the radiant sky temperature below ambient air temperature has been calculated using hourly TMY weather data from 193 stations in the continental United States. The results are plotted in the form of monthly contour maps (Figure 4). The reader is advised to use caution in interpolating between contour lines, especially near seacoasts and mountain ranges. The following observations can be made regarding the monthly average sky temperature depression:

1. The average sky temperature depressions below the ambient air temperature always lie within the range of 6 to 24^{o}C (11 to 43^{o}F) throughout the continental United States.
2. The largest depressions are located in the inland southwestern portion of the country
3. The maximum depression from November through June is centered in Arizona and New Mexico, and shifts northward to Nevada and Northern California during the later summer months.
4. In the eastern half of the country the average depression in the winter for a given location is approximately 2 to 6^{o}C (4 to 11^{o}F) greater than the corresponding summer value.
5. In the eastern half of the country the average depression in the north is 2 to 6^{o}C (4 to 11^{o}F) greater than along the Gulf of Mexico for a given month, with the lower values being characteristic of the summer months.

The sky temperature depression as defined by Equation (7) is characterized by a relatively weak dependence on the ambient air temperature, but depends strongly on the variation of ϵ with changes

in dewpoint temperature and cloud cover. This can be illustrated quantitatively by comparing the features of contour maps for the average monthly dewpoint[9] and average opaque sky cover[10] with the sky temperature depression maps presented here.

During the months of October through May, such a comparison shows that the Arizona-New Mexico region has the lowest average cloud cover (0.1 - 0.2 opaque sky cover), while these clear conditions extend northward through California and Nevada during the summer. This is consistent with the sky temperature depression observations 2 and 3. However, one must not expect a close correlation between opaque cloud cover and average sky temperature depression in all instances since the dewpoint temperature also strongly influences the value of the sky temperature. In general, the areas of maximum sky temperature depression shown in the accompanying maps have both clear skies and low dewpoint temperatures. Conversely, the gulf coast region has a moderate to large amount of cloud cover and consistently high dewpoint temperatures throughout the year. These two extreme sets of conditions are reflected by the locations of the maxima and minima in the sky temperature depression maps.

Observations 4 and 5 reflect the interplay between the sky radiance originating with cloud cover and with the amount of atmospheric water vapor over a wide geographical region, and are not as obvious as those relating to the extreme conditions. In general, the gradient of the dewpoint temperatures from north to south is much steeper in winter than during the summer, while the average amount of opaque sky cover increases to a maximum during the winter in the Great Lakes region. The large amount of winter cloud cover around the eastern Great Lakes offsets low dewpoint temperatures to the extent that the sky temperature depression varies only slightly from north to south during that season. On the other hand, the average winter opaque sky cover does not change much from the Texas coast to the Montana border, which gives rise to the larger difference in sky temperature depression over this path.

Calculations of the sky temperature depression have been made previously by Atwater and Ball[11], who generated contour maps on the basis of results from eleven locations. A comparison of their results with ours shows that in most cases we obtain larger sky temperature depressions, typi-

cally by 2-4°C (4-7°F). A difference of 3°C roughly corresponds to a variation in the net radiative flux of 15 W/m^2, which is consistent with the approximations we and they have made. In one instance, however, the sky temperature depressions we obtain are significantly greater than the values calculated by Atwater and Ball. Wintertime values in the northern plains states are reported by them to be 6°C, whereas the values we obtain during the same months are about 14°C (25°F) for this region. Both sets of values are in close agreement around the eastern Great Lakes region, which is encouraging since the three stations used for validation of their model are located near Lake Ontario. Reference to the long term average opaque cloud cover data[10] shows that this region is significantly more cloudy than the northern plains states. Considering the lower dewpoint temperatures of the plains region one would expect a measurably larger sky temperature depression there in the winter than around the eastern Great Lakes, which is consistent with our model.

Although the model on which our results are based differs substantially from that used by Atwater and Ball, we believe that differences arising from the calculation of clear sky radiation by both methods are not sufficient to account for the spread in values reported in the northern plains states. A possible explanation for the discrepancy in sky temperature depression values in this region lies in the different methods of handling the radiative effects of cloud cover. The lowest default cloud layer used by Atwater and Ball is at 950 mb, corresponding to approximately 0.5 km. This is considerably lower than our 2 km default height for low clouds, and would produce the type of discrepancy observed between the two studies. The average monthly winter opaque sky cover over the entire northern U.S. border exceeds 5 tenths, which implies that a value for ceiling height is recorded hourly much of the time on the TMY weather tapes (when sky cover $\geq$ 0.6). In the method used by us to calculate the radiation emitted from cloud bases, we use the recorded ceiling height when available. This reduces the dependence on a default cloudbase height, especially in regions of heavy overcast, such as the one in question.

5. *SELECTIVE SKY TEMPERATURE DEPRESSION*

The conventional sky temperature is defined as the temperature of a horizontal blackbody surface in radiative equilibrium with the sky and isolated from all other heat paths. An analogous definition can be stated for the selective sky temperature as the temperature of a horizontal spectrally selective surface in radiative equilibrium with the sky. The effective selective sky temperature depends on the spectral emissivity of the radiator surface, $\epsilon_r(\lambda)$. In order to quantify the definition for selective sky temperature, we write the condition for equal incoming and outgoing radiative power for a horizontal radiating surface exposed to the sky as

$$\int_o^\infty d\lambda \epsilon_r(\lambda)\, R(\lambda) = \int_o^\infty d\lambda \epsilon_r(\lambda)\, B_{T^*_{sky}}(\lambda), \tag{8}$$

where $R(\lambda)$ is the spectral intensity of the hemispherically averaged incident sky radiation, and $B_{T^*_{sky}}(\lambda)$ is the Planck distribution function for a blackbody at temperature T^*_{sky}. Eq. (8) defines the effective sky temperature T^*_{sky} for the selective radiator. The selective sky emissivity ϵ^* is defined as the ratio of the incident radiative power from the sky to the power that would be received from a blackbody at ambient air temperature T_{air},

$$\epsilon^* = \frac{\int_o^\infty d\lambda \epsilon_r(\lambda) R(\lambda)}{\int_o^\infty d\lambda \epsilon_r(\lambda) B_{T_{air}}(\lambda)}. \tag{9}$$

Equation (8) then allows one to write

$$\epsilon^*\, B(T_{air}) = B(T^*_{sky}), \tag{10}$$

where $B(T) = \int_o^\infty d\lambda \epsilon_r(\lambda) B_T(\lambda)$.

The usefulness of equation (10) is twofold: the quantities $B(T_{air})$ and $B(T^*_{sky})$ can be obtained readily from tables of integrals of Planck functions [12] when the selective radiator emissivity approximates a step function, and values for ϵ^* have been measured by us for a surface having a high emissivity only between 8.1 and 13.7 microns. The latter condition represents a nearly ideal selective surface for radiative cooling applications. The selective sky emissivity ϵ^* is related to the familiar blackbody sky emissivity ϵ by means of the expression [see Equation (11) and Table 1 of Reference 3],

$$\epsilon^* = -0.034 - 0.773\, \epsilon + 1.807\, \epsilon^2. \tag{11}$$

Evaluating Equation (10) for $\epsilon(\lambda)=1$ one obtains the blackbody sky emissivity

$$\epsilon = (T_{sky}/T_{air})^4. \tag{12}$$

Here, T_{sky} is the blackbody sky temperature and T_{air} is the ambient air temperature.

We have used values for T_{sky} together with T_{air} = 20°C and 40°C, corresponding to sky temperature depressions ΔT_s between 0 and 30°C. The resulting values of ϵ obtained from Equation (12) are used in Equation (11) to calculate ϵ^* . Substitution of this value into equation (10) enables us to calculate T^*_{sky} and the selective sky temperature depression ΔT^*_s . The result of this process is shown in Figure 5. It is remarkable, and very convenient, that the relationship between the sky temperature depressions for an 8 to 14 micron selective radiator and a blackbody radiator is nearly linear. *The selective sky temperature depression is thus obtained from the contour maps of Figure 4 simply by multiplying the contour values by a factor of 2.4!*

6. *MONTHLY DISTRIBUTION OF "COOL" SKY TEMPERATURES*

The monthly sky temperature depression contour maps presented in Section 4 are not sufficient by themselves to enable prediction of the performance of a radiative cooling system. Even if a large sky temperature depression is available, the radiant temperature of the sky may be too high to allow it to act as an effective heat sink if the ambient air temperature is excessive. Such a situation occurs during July and August in the desert area of the southwest. Conversely, in some locations having a modest sky temperature depression, the air temperatures may be moderate enough so that radiative cooling can satisfy at least part of the cooling load.

Reliable performance predictions are, of course, highly system specific, as well as being dependent on the temperature of the sky and the ambient air. In an attempt to provide information regarding the radiant sky cooling resource while avoiding the specificity of a particular radiative system we adopt the following procedure. For a radiative cooling system to effectively maintain comfort in a building, the temperature of the emitting surface must remain below the desired comfort level. Even if the emitter is directly coupled radiatively to the living space (i.e., if the ceiling is in direct contact with the emitter) it is doubtful that it can provide adequate cooling if its surface tem-

perature exceeds 20-22^{o}C (68 - 72^{o}F). The sky temperature in turn must be lower than the radiative surface temperature by an amount that depends both on the ambient air temperature and on the cooling system characteristics.

As an approximate limiting case of marginal radiative cooling we consider a system using a white painted emitter with a conventional polyethylene glazing in a region having a 10^{o}C (18^{o}F) average sky temperature depression[13]. If the nighttime ambient air temperature is 26^{o}C (79^{o}F) then the surface can lose heat at a rate of approximately 17 W/m^{2} if convective heat intrusion is adequately suppressed and a radiator temperature of 22^{o}C is maintained. Improvements in selective radiator and glazing materials will significantly improve this marginal cooling performance, as would the availability of a greater sky temperature depression. Under these approximately "limiting" conditions the sky temperature is 16^{o}C (61^{o}F).

Although the emphasis of this paper is to present information on the radiative cooling resource, rather than on system-specific cooling load characteristics, it is of interest to relate the proposed T_{sky} <16^{o}C condition to cooling loads calculated for radiatively cooled buildings. Clark [14] has computed the total cooling load for a dry roofpond residence operated so as to take advantage of radiative cooling, and has compared this to the total cooling load of a similar energy conserving building having no passive cooling system. The difference between these two values is attributable to the fraction of the total cooling load of the building which is satisfied by a radiative cooling system. In Figure 6 we plot this fraction as a function of the total number of hours during June, July, and August for which T_{sky} is less than 16^{o}C. The two cities not shown on this graph, Bakersfield, CA and Dodge City, KS could not be plotted since the TMY data sets were incomplete for the required three month period. A second set of points is also plotted in Figure 6, which represent preliminary results from a Passive Cooling Technology Assessment performed at Lawrence Berkeley Laboratory [15]. The system modeled in this case is a single story low mass office building having an air plenum in contact with a metal roof which acts as a radiative cooling surface. No attempt was made to optimize the radiative cooling system in this case, and thermal storage beyond the conventional structural components of the building was not included. This fact, coupled with the day-

time use pattern typical of office buildings, accounts for the lower predicted performance of this system in comparison to the more nearly ideal configuration of the roofpond building. The point we wish to emphasize here is that the fraction of the total load satisfied by radiative losses to the sky is reasonably represented by straight line fits through the origin, indicating that the suggested criterion ($T_{sky} < 16^{o}C$) is a reasonable one to use for drawing preliminary conclusions regarding the efficacy of radiative cooling systems.

In order to provide an overview of the percentage of time during which the sky temperature is less than $16^{o}C$ we have calculated the number of hours per month when this condition is satisfied for 193 TMY data sites. The results are plotted in the form of contour maps for the months of May through September (Figure 7).

7. *SKY TEMPERATURE DISTRIBUTIONS*

Both the sky temperature and its depression below the ambient air temperature are important quantities for assessing the feasibility of cooling with a radiative system. The averages of these quantities have been presented in the form of contour maps in Sections 4 and 6. It is also desirable to have access to additional statistical information for a given climate site. In this section we develop two such distributions.

The sky temperature depression can be considered a weighted measure of the effects of atmospheric humidity and cloud cover. The effect of diurnal air temperature fluctuations is largely removed by subtraction. Since the cooling of buildings occurs at and below the ambient air temperature, the sky temperature depression provides one convenient parameter for judging the potential for cooling with radiative systems. If this difference is less than about $10^{o}C$ it is unlikely that the sky will be able to act effectively as a radiative heat sink for cooling near ambient temperatures. On the other hand, a difference of 15^{o} to $20^{o}C$ should enable a significant amount of heat to be removed by a properly designed system. The fraction of hours having sky temperature depressions within $1^{o}C$ intervals between 0^{o} and $30^{o}C$ is plotted in histogram form for the summer months at three locations (Figure 8a). An example of a good radiative cooling climate is Fresno, CA in which the depression

is almost always greater than 15°C (27°F) during overheated periods. An extremely unfavorable climate for radiative cooling is illustrated by by Miami, FL. Here the sky temperature depression seldom exceeds 10°C (18°F), and typically lies between 4° and 9°C (7 and 16°F). An intermediate example is shown for Phoenix, AZ in which the months of July and August are characterized by moderate to large sky temperature depressions, with even more favorable conditions occurring during early summer and September.

At first glance the monthly sky temperature depression histograms for Phoenix do not appear to be obviously less favorable for radiative cooling than those of Fresno, which has been characterized as a good radiative cooling climate. The reason why Fresno is a better location for radiative cooling is that in Phoenix during the summer months even a large sky temperature depression is unable to cause the sky temperature to become low enough to be used for cooling buildings, due to the high nighttime ambient air temperatures. To illustrate this point and to enable further comparisons we have plotted graphs showing the percentage of hours each month for which the sky temperature falls below values ranging between 10° and 26°C (Figure 8b). In Fresno it is seen that even during the mid summer months the sky temperature remains below 10°C half the time. In contrast, for the same months Phoenix spends only about 5% of the time in this condition. The infeasibility of using radiative cooling in Miami during the summer with existing blackbody radiator systems is also demonstrated by Figure 8b, from which it is apparent that cool (~10°C) sky temperatures are never achieved during the hottest months, and for more than half the time the sky temperature exceeds 21°C (70°F).

Additional graphs of both types are presented in Figures 9 - 11 to aid the reader in evaluating the potential for radiative cooling in a range of additional U.S. climates. It must be stressed here that the emphasis of this paper is on the characterization of the radiative cooling *resource*. The performance of actual systems will also depend very strongly on the configurations and engineering details of these systems. A detailed performance evaluation can only be made by system simulation studies and the construction of real radiative cooling systems, few of which exist to date.

8. *APPENDIX: SIMPLIFIED MONTHLY SKY EMISSIVITY CALCULATION METHOD*

The following method has been developed to permit estimation of the magnitude of year-to-year fluctuations in the monthly average sky emissivity. It is based on average monthly values for the drybulb temperature, dewpoint temperature, and for tenths of total sky cover measured between sunrise and sunset. Daytime sky cover is used instead of 24 hour sky cover because nighttime data are not as readily available. The generalized form for the total sky emissivity is given by Equation (5) of Section 2. We make the simplifying assumption that the quantity

$$\Sigma_i \; n_i \epsilon_{c,i} \; \Gamma(h_i)$$

can to first approximation be replaced by the simple product $N\,\Gamma$, where N is the fractional monthly average of the sky cover between sunrise and sunset. Γ is then a number which combines the contribution to the sky emissivity from clouds of various emissivities occurring at various cloudbase heights throughout the month. We then make the assumption that Γ is characteristic of the cloud pattern for a specific month at a given location. The simplified equation to be solved is:

$$\epsilon = \epsilon_o + (1 - \epsilon_o) N \Gamma. \qquad \text{(A1)}$$

To estimate the value of Γ we use this equation with monthly average values of ϵ, ϵ_o, and N calculated from hourly TMY weather data. The resulting values for Γ are shown in Table A1 for the five locations at which calculations have been carried out.

Once values for Γ are obtained, we make the further assumption that this value is essentially constant from year to year at a given geographical location. The cloud amount N may change considerably, but the mix of cloud heights and emissivities is assumed to remain approximately constant for the same month of any year. Using these calculated monthly values for Γ we obtain the required average weather parameters for specific years from the Local Climatological Data (LCD) Summaries published by the U.S. National Weather Service [16]. Equation (1) of Section 2 is used to calculate the average clear sky emissivity and the quantity N is obtained directly from the monthly LCD summary.

In order to esti validity of the simplified LCD calculation procedure, values for ϵ have been calculated for s 1967 through 1981 at Tucson, AZ, West Palm Beach, FL, and San Antonio, TX. The resulyear averages were then compared to the average monthly emissivity obtained from calculatiol on hourly TMY data. The average standard deviation of calculated monthly LCD sky emissrom the corresponding TMY values is $\pm$ 0.02 in Tucson and San Antonio, and $\pm$ 0.012 in W Beach. Except for two months in San Antonio (May and October) the TMY and mean LCDalways lie within one standard deviation of each other.

The standard d in monthly total sky emissivity also furnishes an answer to our original question regarding ical year-to-year fluctuations of this quantity. The average standard deviation for monthly Lemissivities is $\pm$ 0.02 in Tucson and San Antonio, and $\pm$ 0.012 in West Palm Beach.

9. *REFEREN*

1. *A Fundamentals,* pp. 26.3-26.6, American Society of Heating, Refrigerating, anonditioning Engineers, Atlanta (1981).

2. H and J. I. Yellott, Natural air conditioning with roof ponds and movable insula*SHRAE Trans. 75* pp. 165-177, also see pp. 178-190 (1969).

3. M and P. Berdahl, Summary of results for the spectral and angular sky radiatiurement program. Submitted to *Solar Energy* (1983).

4. Phl and M. Martin, Emissivity of clear skies. Submitted to *Solar Energy* (1

5. P.l and R. Fromberg, The thermal radiance of clear skies. *Solar Energy 29* pp. 22982).

6. D and G. Jurica, Effective atmosphere emissivity under clear skies. *J. Appl. M* pp. 349 (1972).

7. F. X. Kneizys, *et al.*, Atmospheric Transmittance/Radiance: Computer Code LOWTRAN 5. *U.S. Air Force Geophysics Laboratory*, Hanscom AFB, Massachussetts, AFGL-TR-80-0067.

8. C. Platt and A. Dilley, Remote sounding of high clouds. IV: Observed temperature variations in cirrus optical properties. *J. Atmos. Sci. 38* pp. 1069 (1981).

9. *Climatic Atlas of the United States.* U.S. Department of Commerce, National Climatic Center, Asheville, NC, pp. 57-58 (1979).

10. *Solar Radiation Energy Resource Atlas of the United States.* Solar Energy Research Institute, Superintendent of Documents, U.S. Government Printing Office, Washington, DC 20204 (1981).

11. M. Atwater and J. Ball, Computation of IR sky temperature and comparison with surface temperature. *Solar Energy 21* p. 211 (1978).

12. J. A. Duffie and W. A. Beckman, *Solar Energy Thermal Processes*, p. 68. Wiley, New York (1974).

13. M. S. Kruskopf, P. Berdahl, M. Martin, F. Sakkal, and M. Sobolewski, Radiative cooling test facility and performance evaluation of 4 mil aluminized polyvinyl fluoride and white paint surfaces. Lawrence Berkeley Laboratory Report, LBL-12049 (1980).

14. G. Clark, Passive/Hybrid comfort cooling by thermal radiation. *Proceedings of the International Passive and Hybrid Cooling Conference*, Miami Beach, p. 709 (1981).

15. W. L. Carroll, *et al.*, Passive cooling strategies for nonresidential buildings: An impact assessment. Lawrence Berkeley Laboratory Report, LBL-14558 (1982).

16 *Local Climatological Data.* National Climate Center, NOAA, U.S. Department of Commerce, Asheville, NC.

FIGURE CAPTIONS

Figure 1: Cloud factor Γ as a function of cloudbase height. The exponential curve is described by $\Gamma = \exp(-h/h_o)$ where $h_o = 8.2$ km.

Figure 2: Average hemispherical cloud emissivity for 22 high cloud systems derived from Platt and Dilley[8]. The sloped straight line is a least squares fit to the plotted points. Emissivities less than 0.15 are assumed to correspond to clouds not visible to an observer.

Figure 3: Cloud factor Γ as a function of cloudbase temperature depression $\Delta T_c = T_{air} - T_{cloud}$. The exponential curve is described by $\Gamma = \exp(-\Delta T_c/\Delta T_o)$ where $\Delta T_o = 46^o C$.

Figure 4: Contour maps showing the average monthly sky temperature depression $\Delta T_{sky} = T_{air} - T_{sky}$ (^oC).

Figure 5: Selective sky temperature delpression ΔT^*_{sky} plotted as a function of the conventional blackbody sky temperature depression ΔT_{sky} for an air temperature of 30^{o}C.

Figure 6: Calculated fraction of the total summer cooling load satisfied by two types of radiative cooling systems: o= roofpond simulation [14]; Δ= low mass commercial building with unoptimized air transfer plenum below a radiatively cooled roof surface [15].

Figure 7: Contour maps showing the percentage of monthly hours during which the sky temperature lies below 16^{o}C.

Figure 8a: Histogram showing distributions of the sky temperature depression $\Delta T_{sky} = T_{air} - T_{sky}$ as a percentage of monthly hours. The zero point for each month is offset by 10 percent on the vertical scale from neighboring months to enable five months of data to be plotted on a single graph.

Figure 8b: Percentage of monthly hours during which the sky temperature lies below the values 10 to 26°C plotted along the horizontal axis.

TABLE CAPTIONS

Table 1: Measured and calculated average monthly sky emissivities for the 27 month set of data for which each set of monthly measurements is at least 60% complete.

Table A1: Monthly average values for Γ derived from analysis of TMY hourly weather data.

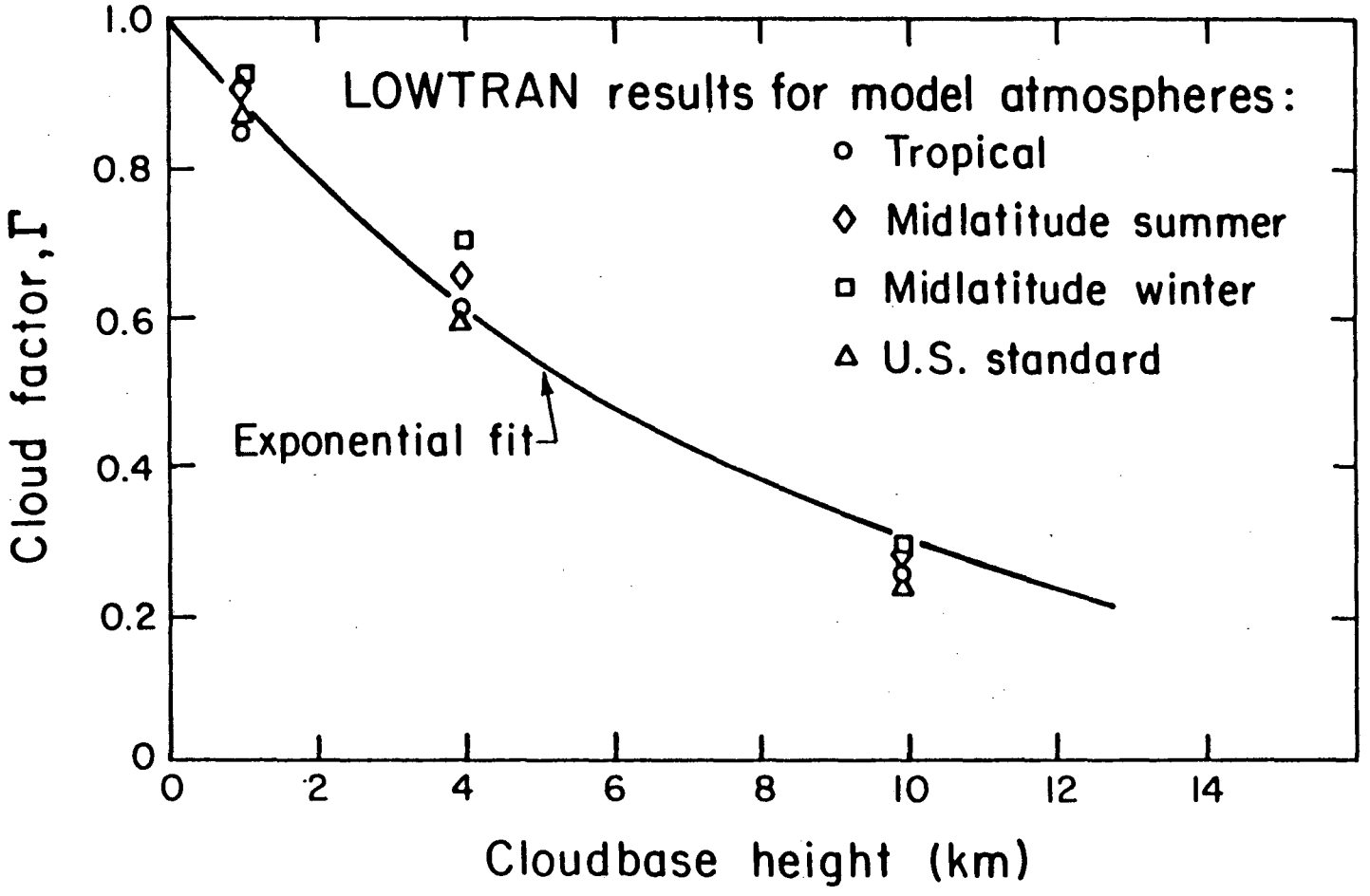

XBL 831 - 56

Figure 1

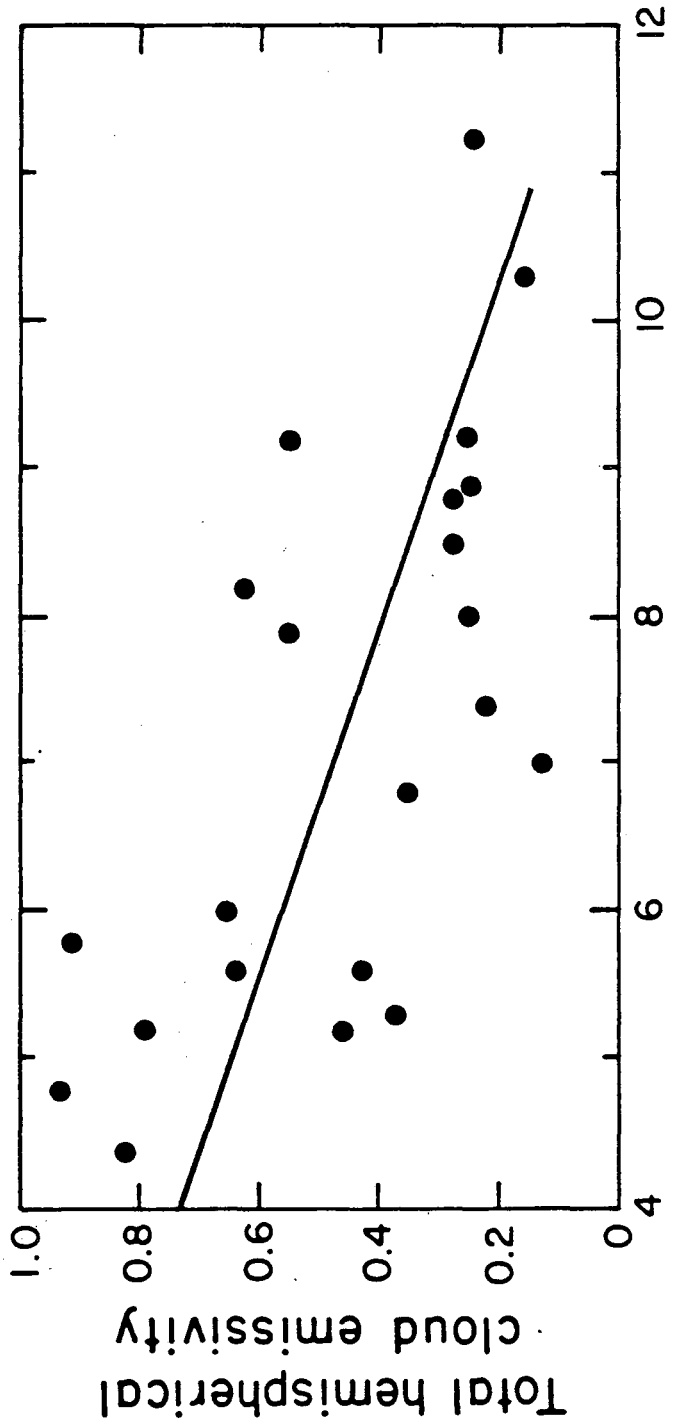

XBL 831-55

Figure 2.

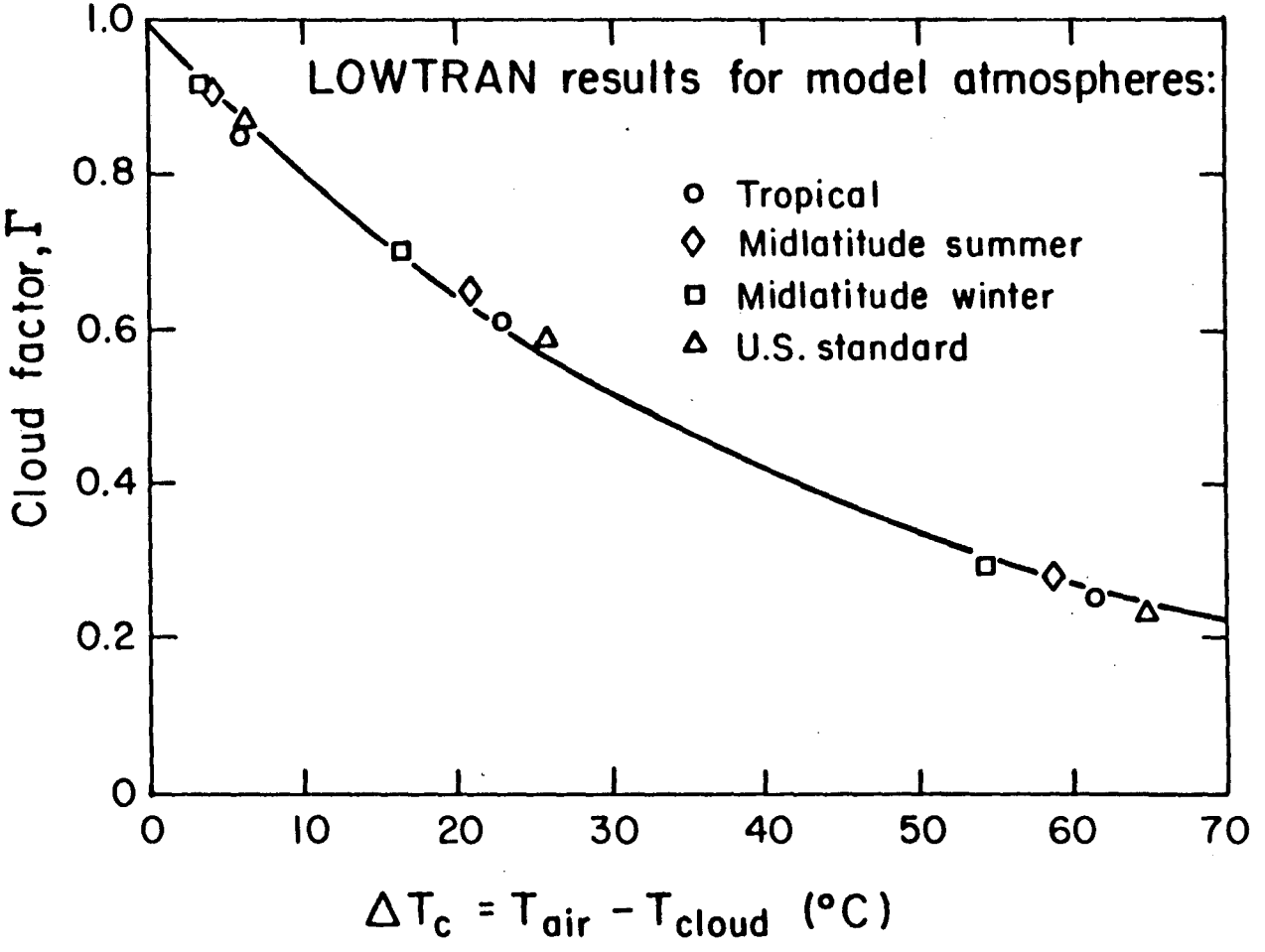

XBL 831 - 57

Figure 3.

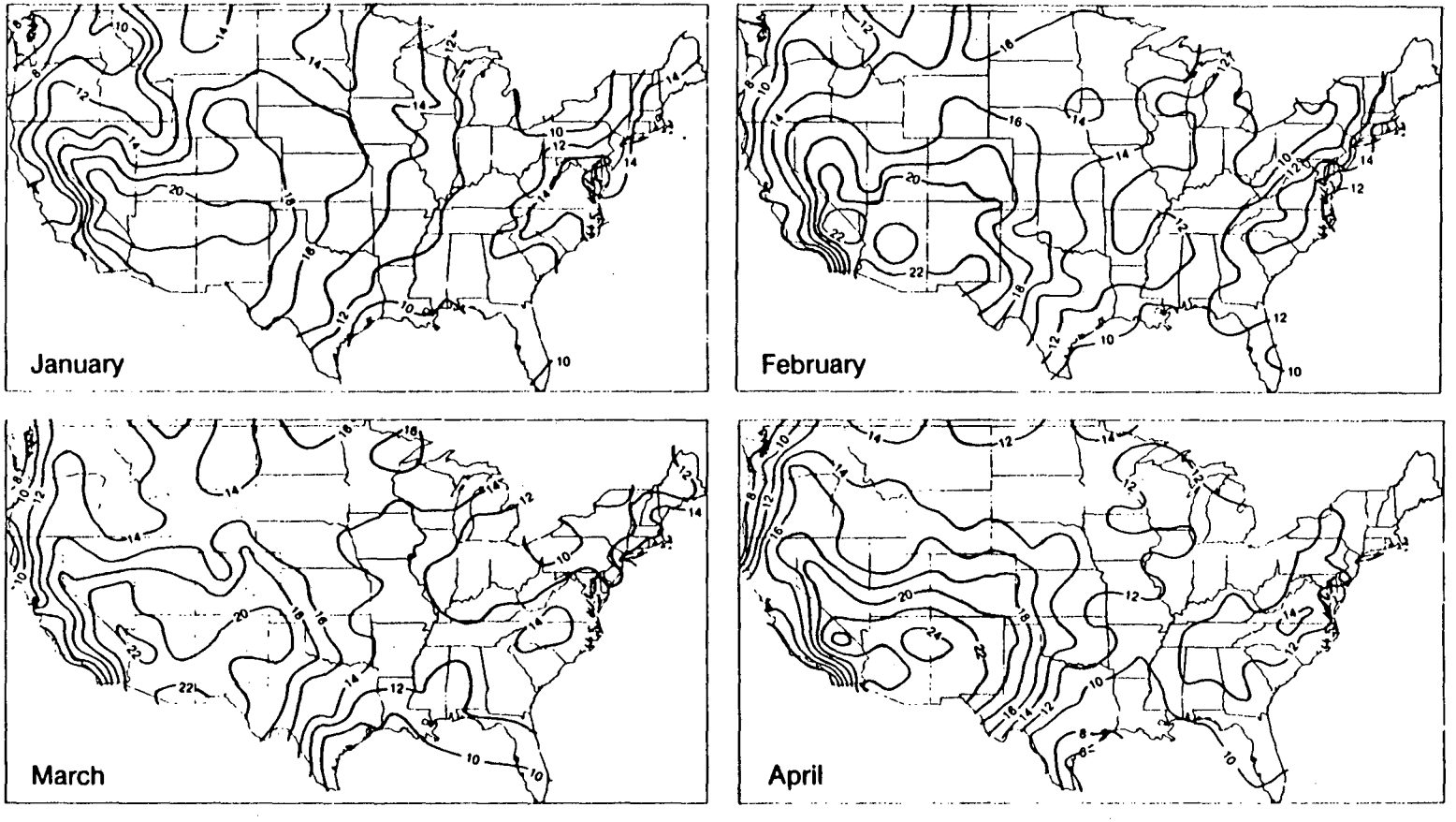

SKY TEMPERATURE DEPRESSION (degrees C)

XBL 833-80

Figure 4a.

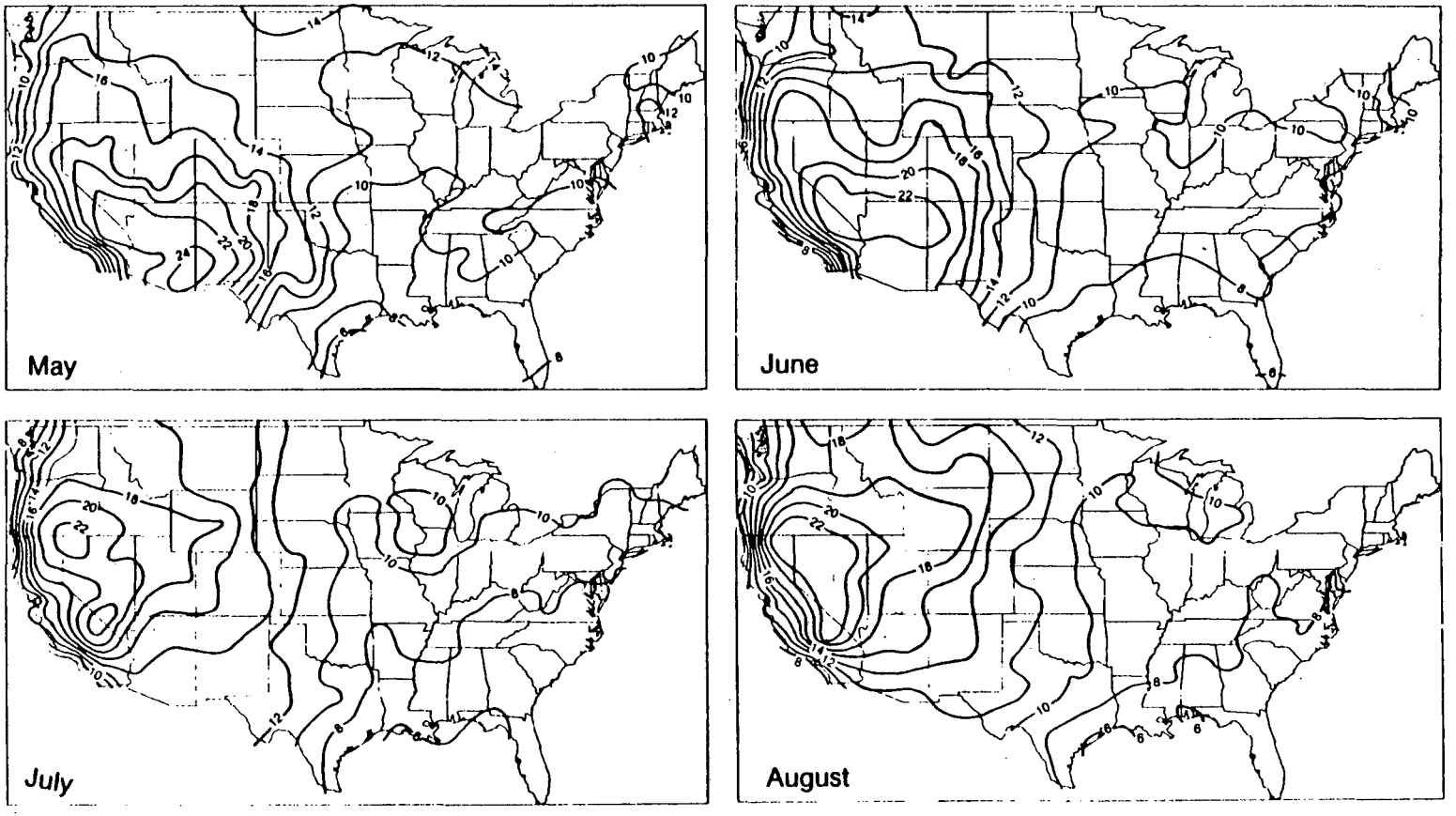

SKY TEMPERATURE DEPRESSION (degrees C)

XBL 833-83

Figure 4b.

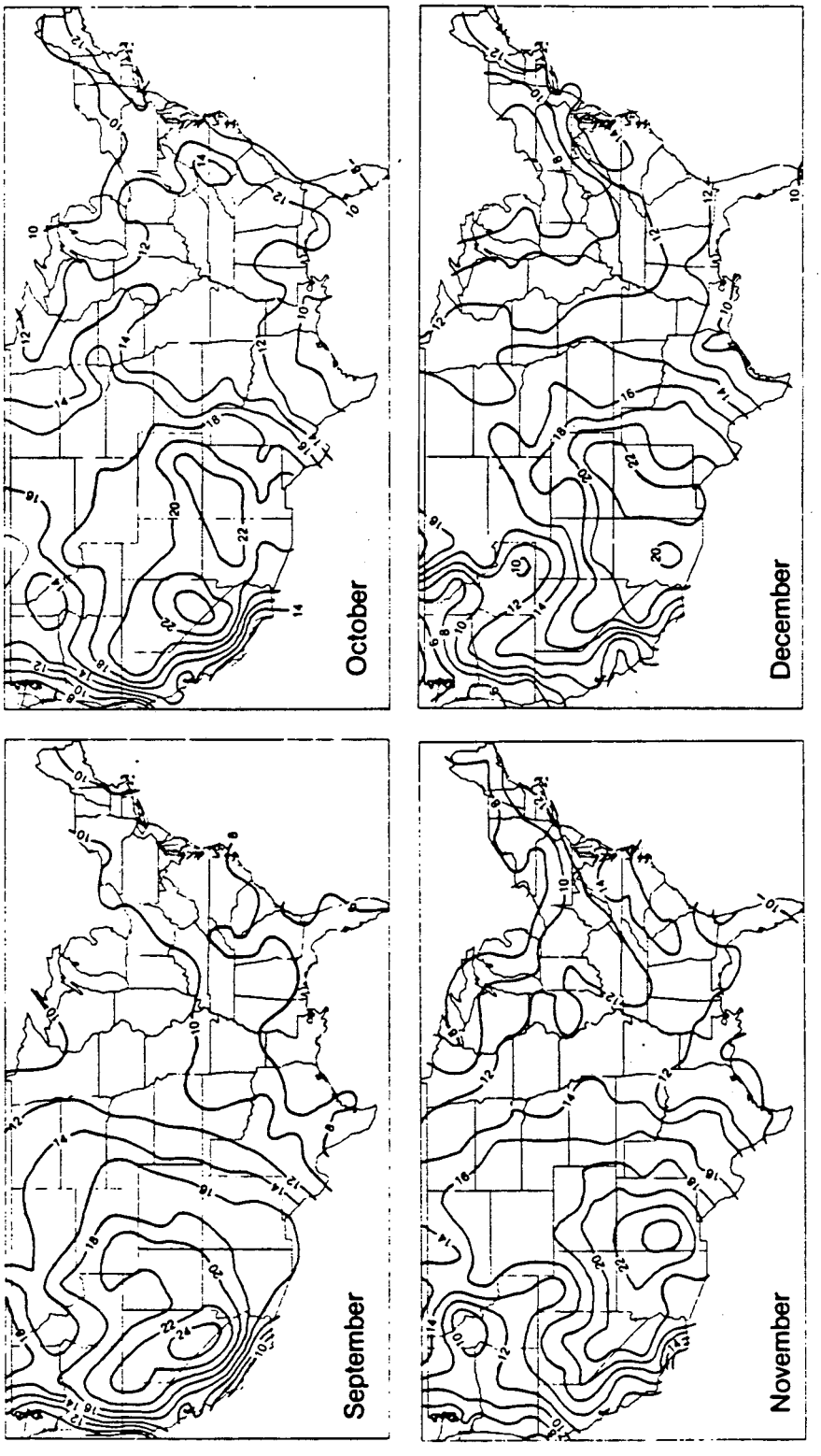
October
December
September
November
SKY TEMPERATURE DEPRESSION (degrees C)
XBL 833-81

Figure 4c.

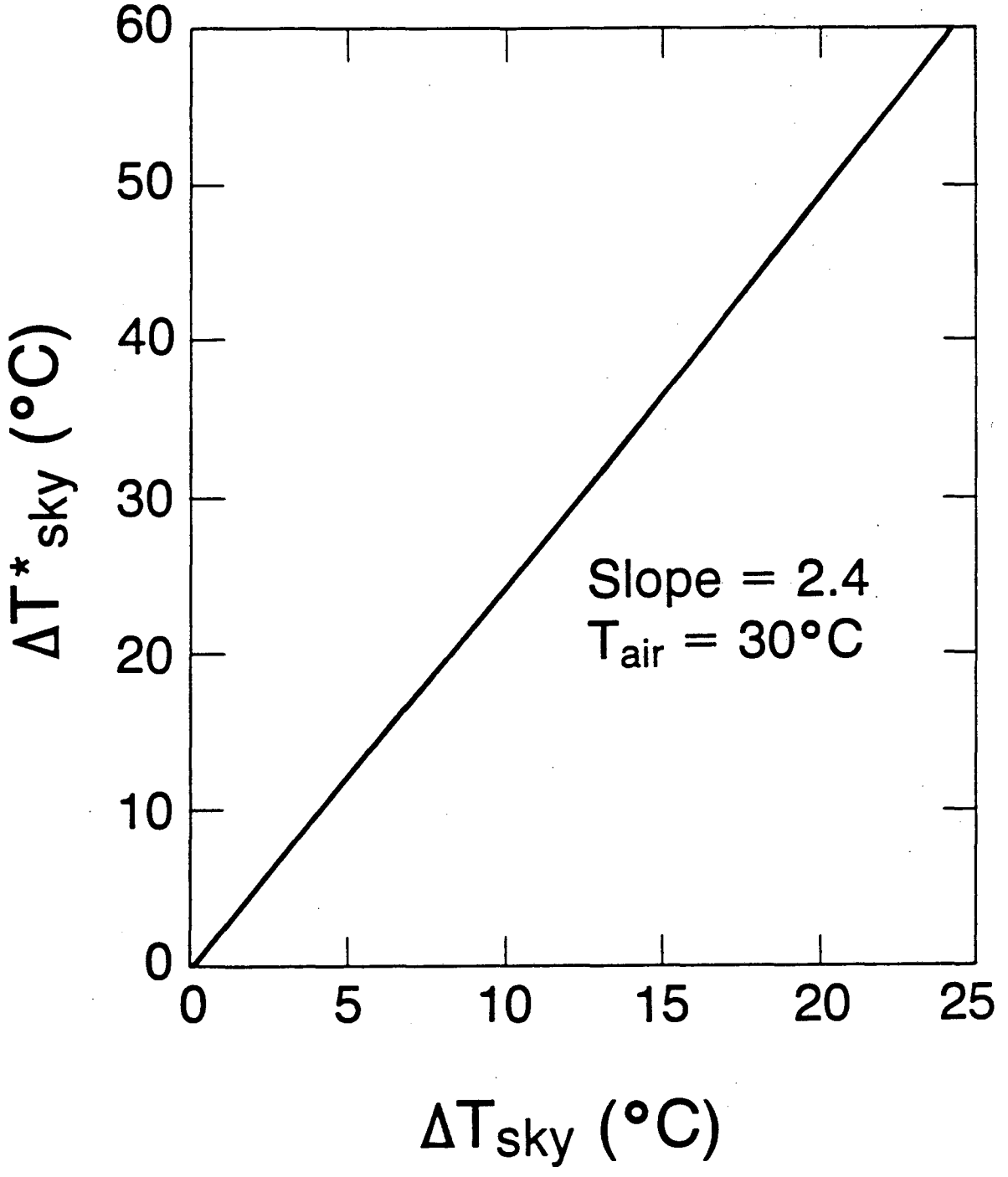

XBL 837-2772

Figure 5.

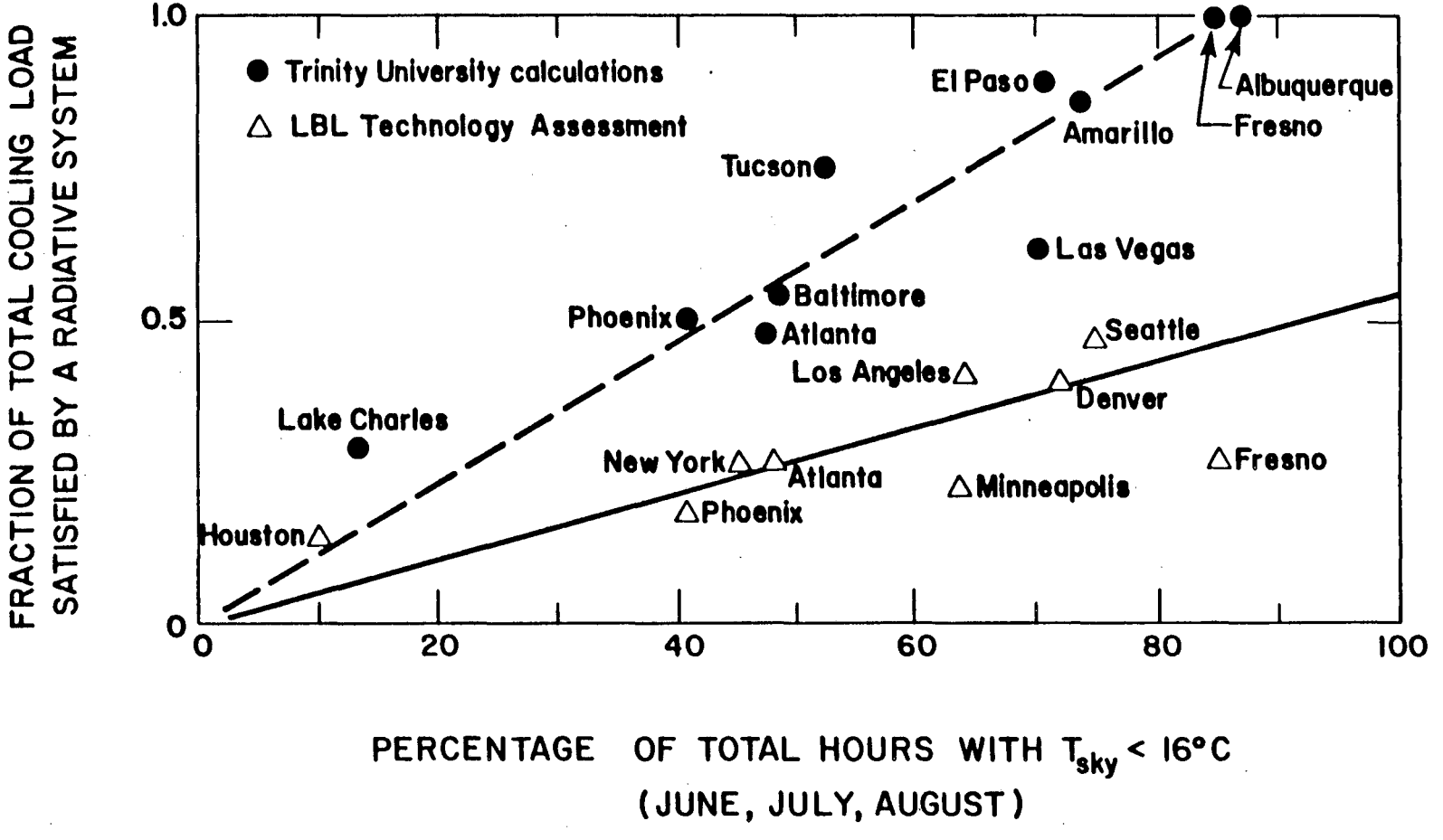

XBL 833-77A

Figure 6.

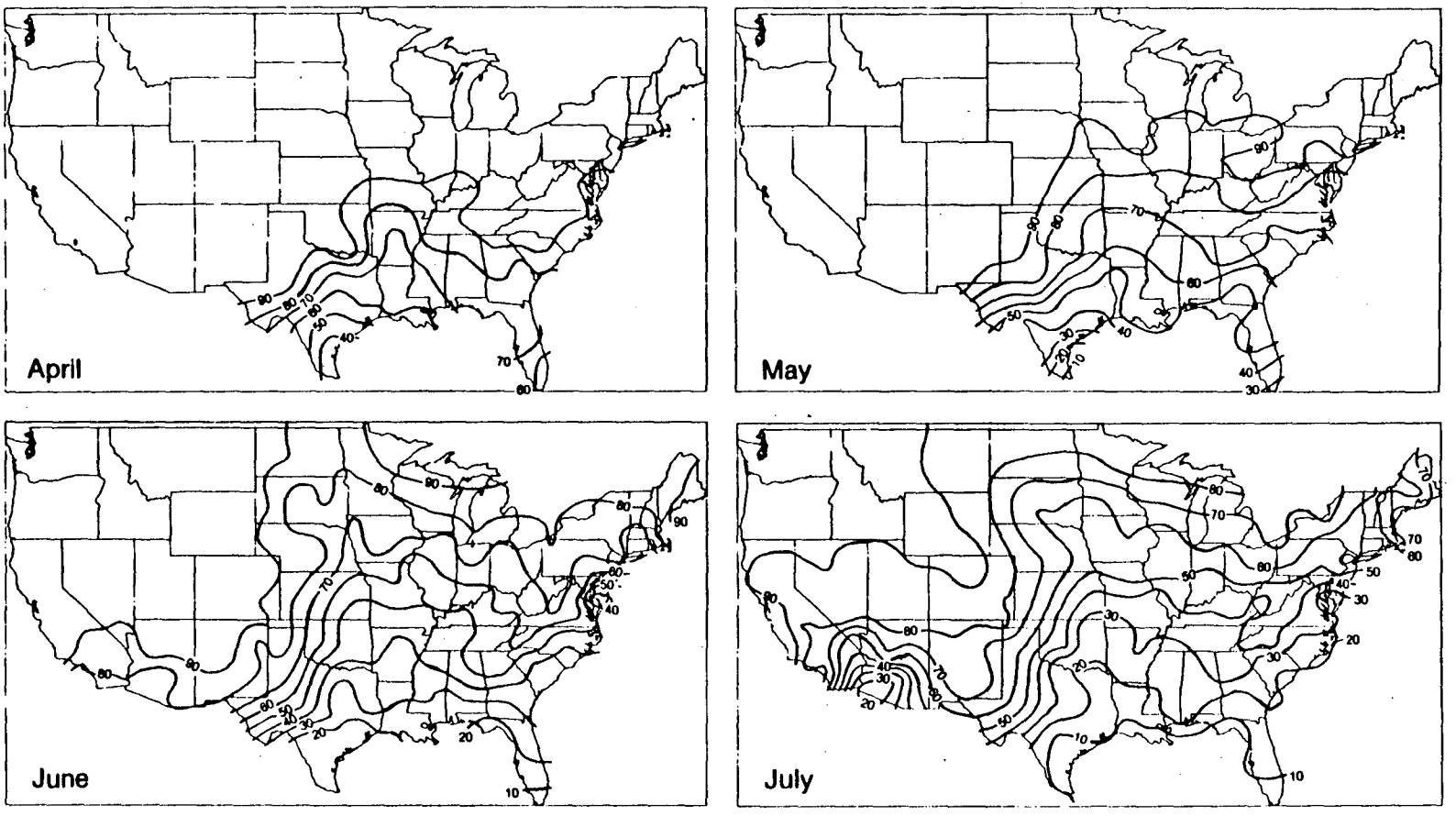

PERCENTAGE OF HOURS WITH SKY TEMPERATURE BELOW 16 DEGREES C.

XBL 833-82

Figure 7a.

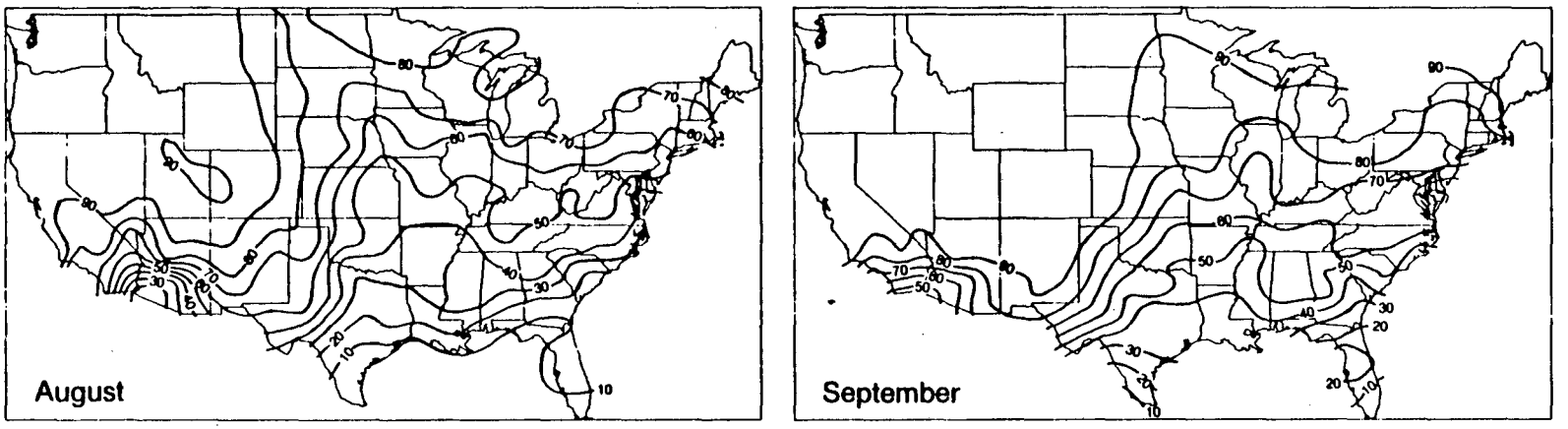

PERCENTAGE OF HOURS WITH SKY TEMPERATURES BELOW 16 DEGREES C.

XBL 833-84

Figure 7b.

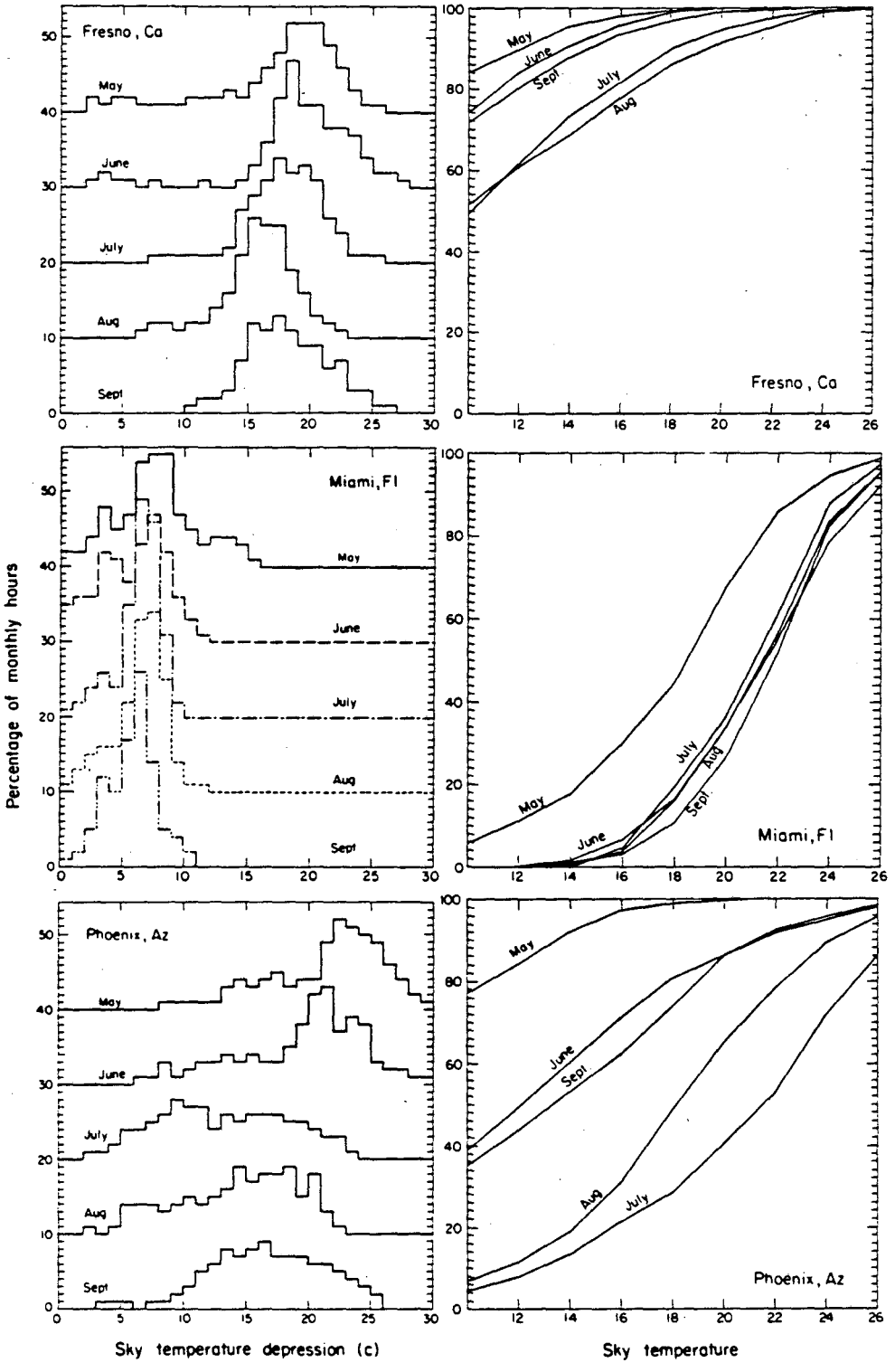

Figure 8a.

Figure 8b.

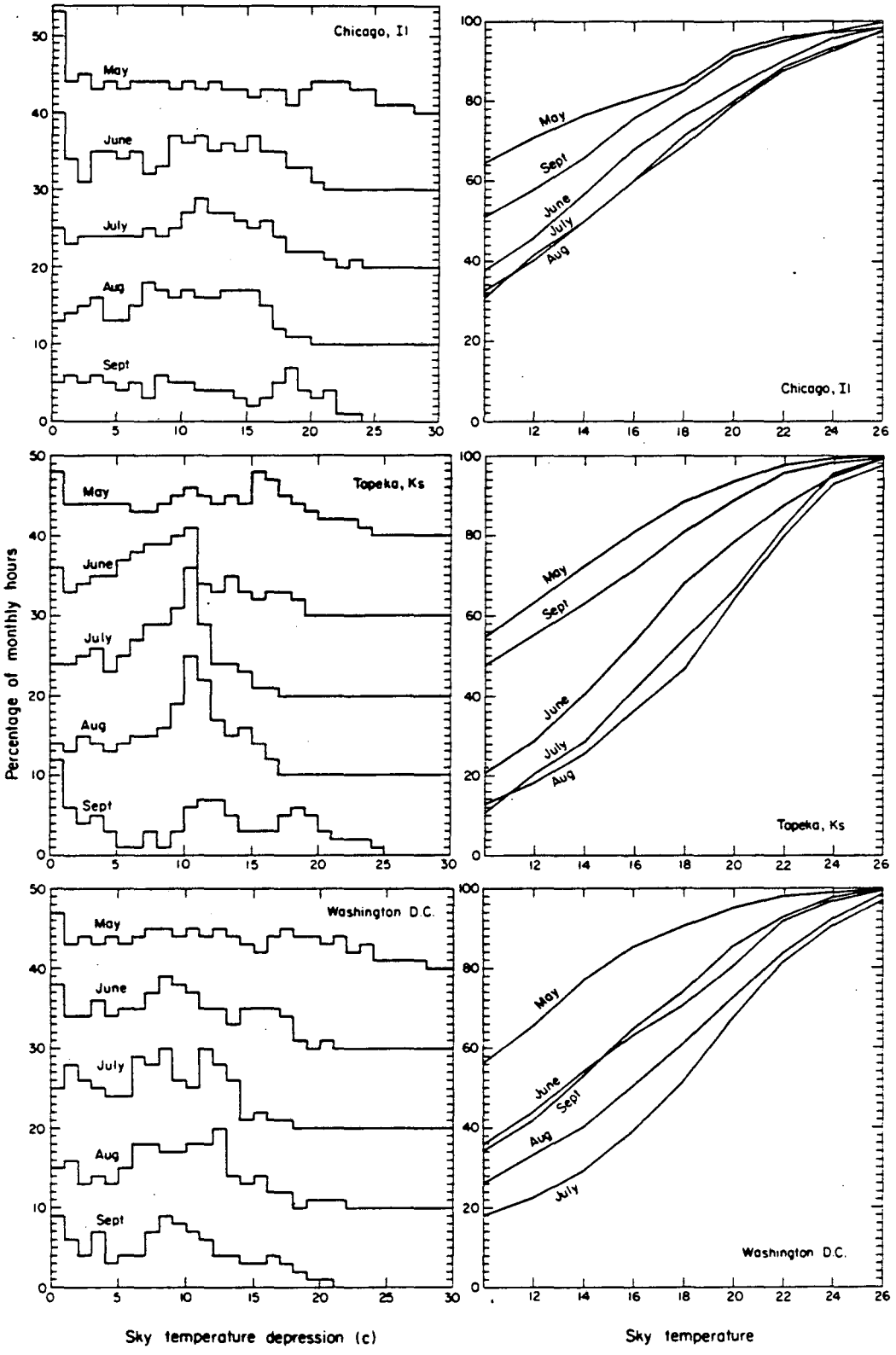

XBL 833-86

Figure 9a.

Figure 9b.

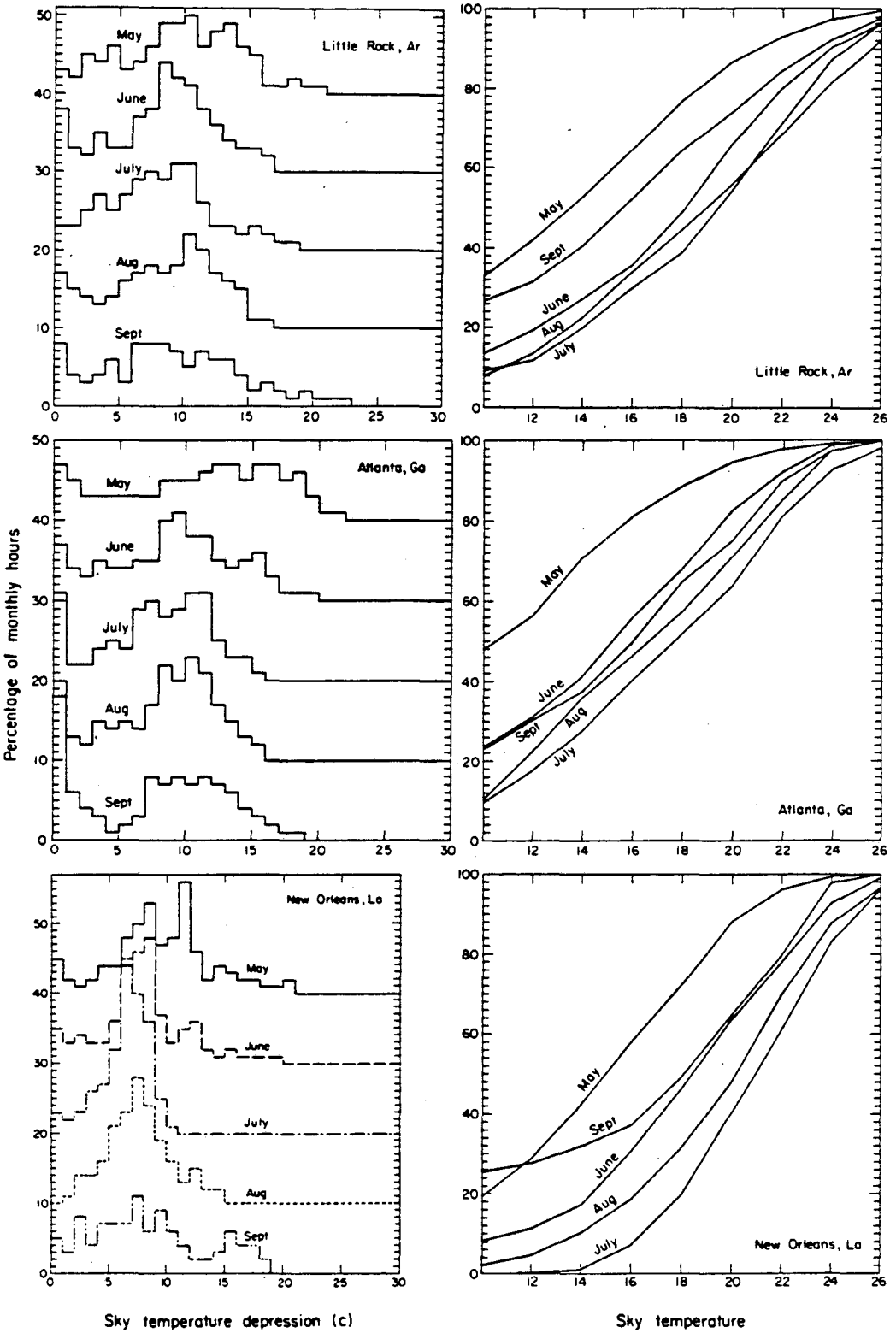

Figure 10a.

Figure 10b.

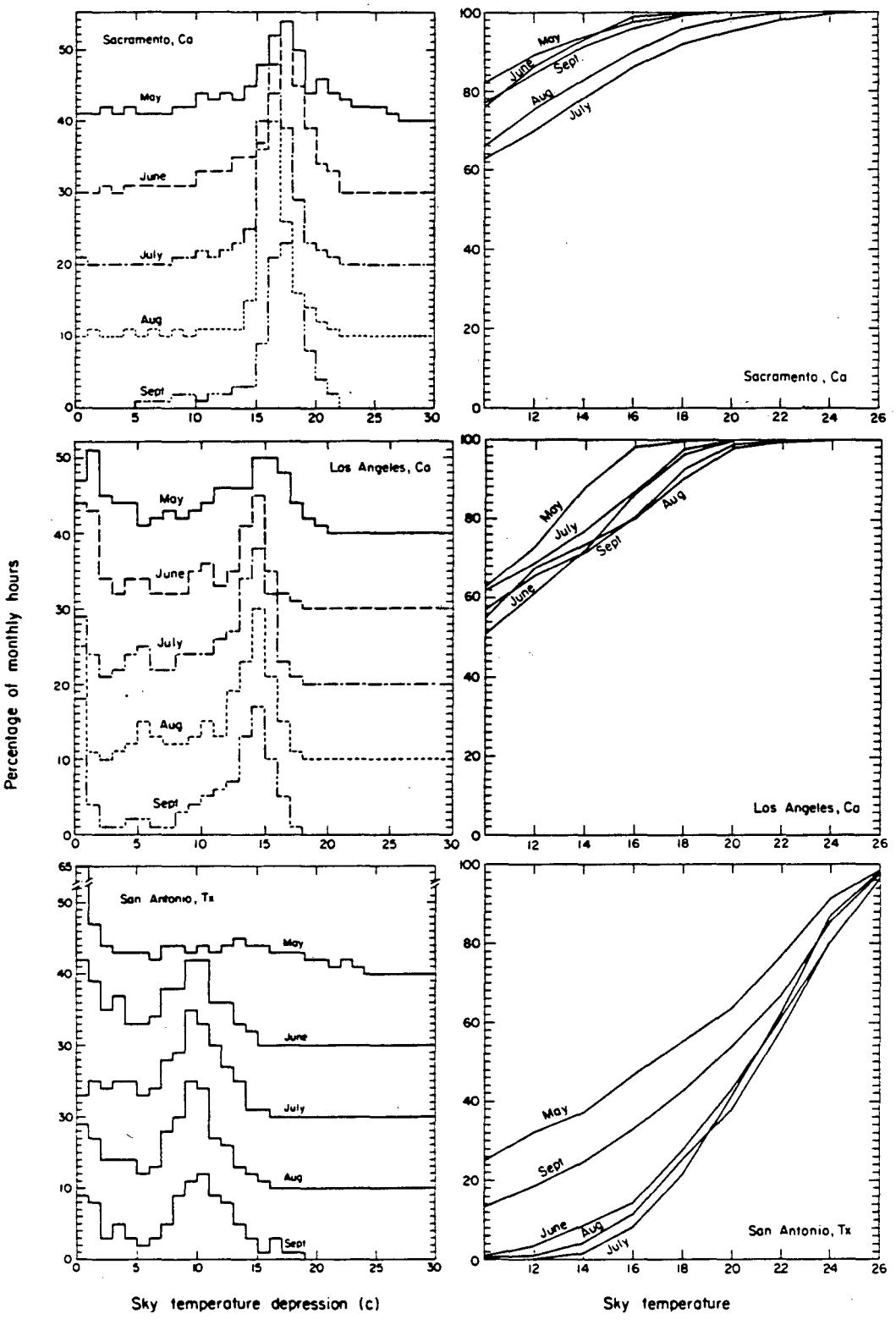

Figure 11a.

Figure 11b.

Table 1: Measured and calculated average monthly sky emissivities for the 27 month set of data for which each set of monthly measurements is at least 60% completed.

City	Month/ Year	% completeness	ϵ_{MEAS}	ϵ_{TMY}	ϵ_{LCD}
San Antonio	7/79	60	0.917	0.895	0.925
	12/79	67	0.853	0.845	0.857
	1/80	83	0.871	0.816	0.852
	5/80	96	0.909	0.896	0.928
	6/80	100	0.879	0.912	0.912
	7/80	60	0.874	0.895	0.881
Gaithersburg	7/79	83	0.919	0.896	0.910
	9/79	85	0.881	0.870	0.888
	10/79	66	0.866	0.826	0.845
	1/80	71	0.849	0.806	0.850
	2/80	83	0.776	0.806	0.776
	3/80	82	0.857	0.803	0.836
St. Louis	9/79	98	0.792	0.865	0.828
	10/79	94	0.809	0.829	0.850
	6/80	75	0.822	0.884	0.879
	7/80	62	0.845	0.891	0.890
	8/80	60	0.838	0.887	0.885
	10/80	78	0.759	0.829	0.809
Tucson	6/79	76	0.772	0.747	0.757
	7/79	93	0.821	0.850	0.861
	8/79	64	0.837	0.855	0.858
	9/79	62	0.795	0.800	0.817
	10/79	78	0.749	0.750	0.767
	12/79	72	0.730	0.736	0.755
	2/80	76	0.781	0.719	0.789
	3/80	96	0.746	0.728	0.766
	4/80	90	0.727	0.717	0.731
Average Emissivity			0.825	0.828	0.841

Table A1: Monthly average values for Γ derived from analysis of TMY hourly weather data.

	Tucson	Palm Beach	San Antonio	Baltimore	St. Louis
Jan	0.3597	0.6209	0.6009	0.7203	0.6735
Feb	0.3540	0.6148	0.7250	0.6666	0.7533
Mar	0.3817	0.6268	0.9052	0.6483	0.7460
Apr	0.2879	0.6456	0.9293	0.6577	0.6218
May	0.2036	0.5339	0.8245	0.7076	0.6443
Jun	0.3397	0.5438	0.9304	0.6605	0.5901
Jul	0.4579	0.5037	0.5797	0.5923	0.5299
Aug	0.4307	0.4491	0.8197	0.6251	0.5624
Sep	0.4720	0.6246	0.7842	0.6256	0.5103
Oct	0.2474	0.6407	0.9617	0.6459	0.6214
Nov	0.3314	0.5844	0.7875	0.6164	0.6771
Dec	0.3295	0.6477	0.6899	0.6521	0.7215

This report was done with support from the Department of Energy. Any conclusions or opinions expressed in this report represent solely those of the author(s) and not necessarily those of The Regents of the University of California, the Lawrence Berkeley Laboratory or the Department of Energy.

Reference to a company or product name does not imply approval or recommendation of the product by the University of California or the U.S. Department of Energy to the exclusion of others that may be suitable.

TECHNICAL INFORMATION DEPARTMENT
LAWRENCE BERKELEY LABORATORY
UNIVERSITY OF CALIFORNIA
BERKELEY, CALIFORNIA 94720